

## Toward Functional $\pi$ -Conjugated Organophosphorus Materials: Design of Phosphole-Based Oligomers for Electroluminescent Devices

Hai-Ching Su,<sup>†</sup> Omrane Fadhel,<sup>‡</sup> Chih-Jen Yang,<sup>†</sup> Ting-Yi Cho,<sup>†</sup> Claire Fave,<sup>‡</sup>  
Muriel Hissler,<sup>‡</sup> Chung-Chih Wu,<sup>\*,†</sup> and Régis Réau<sup>\*,‡</sup>

*Contribution from the Department of Electrical Engineering, Graduate Institute of Electro-optical Engineering and Graduate Institute of Electronics Engineering, National Taiwan University, Taipei, Taiwan 106, and Institut de Chimie, UMR 6509, Université de Rennes 1, Campus de Beaulieu, 35042 Rennes Cedex, France*

Received October 10, 2005; E-mail: regis.reau@univ-rennes1.fr; chungwu@cc.ee.ntu.edu.tw.

**Abstract:** The photophysical, electrochemical, and optoelectronic properties of conjugated systems incorporating dibenzophosphole or phosphole moieties are described. Dibenzophosphole derivatives are not suitable materials for OLEDs due to their weak photoluminescence (PL) in the solid state and the instability of the devices. Variation of the substitution pattern of phospholes and chemical modification of their P atoms afford thermally stable derivatives, which are photo- and electroluminescent. Comparison of the optical properties of solution and thin film of thioxophospholes shows that these compounds do not form aggregates in the solid state. This property, which is also supported by an X-ray diffraction study of three novel derivatives, results in an enhancement of the fluorescence quantum yields in the solid state. In contrast, (phosphole)gold(I) complexes exhibit a broad emission in thin film, which is due to the formation of aggregates. Single- and multilayer OLEDs using these P derivatives as the emissive layer have been fabricated. The emission color of these devices and their performances vary with the nature of the P material. Interestingly, di(2-thienyl)thioxophosphole is an efficient host for the red dopant DCJTb, and devices using the gold complexes have broad emission spectra.

### Introduction

In the past decade, the synthesis of organic  $\pi$ -conjugated materials has been the focus of much work because of their potential applications in electronic and optoelectronic devices.<sup>1,2</sup> This growing interest is mainly due to the possibility of tailoring their physical properties and supramolecular organization via structural variations.<sup>1,2</sup> Predictive structure–property relationships can be established, and the optimization of characteristic properties to suit a desired function is possible via chemical engineering at the molecular level. This thought process is nicely illustrated by the development of advanced electroluminescent

organic materials<sup>2</sup> following the seminal reports of efficient organic light emitting diodes (OLEDs) based on small molecules and conjugated polymers.<sup>3</sup>

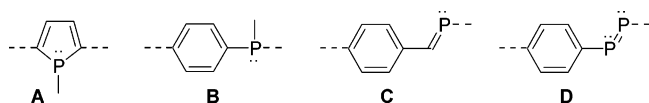
Varying the chemical composition of conjugated systems is thus a major concern to further optimize organic materials. Due to the high flexibility of organic synthesis, many strategies can be envisaged to diversify the structure of  $\pi$ -conjugated molecular materials. The most usual ones imply the synthesis of all-carbon macromolecules incorporating different C-sp<sup>2</sup>- and C-sp-based building blocks (aryle, alkyne, alkene...), and the grafting of substituents with specific properties on these skeletons.<sup>1,2</sup> Another fruitful approach involves the incorporation of heteroatomic moieties into the conjugated frameworks. Nitrogen and sulfur have been intensively used for such a purpose; poly-(aniline)s, poly(pyrrole)s, and poly(thiophene)s are among the most widely investigated  $\pi$ -conjugated systems.<sup>1,2</sup> Organosilicon derivatives such as siloles have also been successfully employed for the construction of efficient molecular materials for optoelectronic applications.<sup>4</sup> In marked contrast, organophosphorus moieties have only recently been considered as potential building blocks for the tailoring of  $\pi$ -conjugated systems.<sup>5</sup> To date, the most widely used phosphorus building block is phosphole **A**

<sup>†</sup> National Taiwan University.

<sup>‡</sup> Université de Rennes 1.

- (1) (a) Müllen, K.; Wegner, G. *Electronic Materials: The Oligomer Approach*; Wiley-VCH: Weinheim, 1998. (b) Martin, R. E.; Diederich, F. *Angew. Chem., Int. Ed.* **1999**, *38*, 1350–1377. (c) Skotheim, T. A.; Elsenbaumer, R. L.; Reynolds, J. R. *Handbook of Conducting Polymers*, 2nd ed.; Dekker: New York, 1998. (d) Nalwa H. S. *Handbook of Conductive Materials and Polymers*; John Wiley and Sons: New York, 1997. (e) Roncali, J. *Chem. Rev.* **1997**, *97*, 173–206.
- (2) For reviews, see: (a) Kraft, A.; Grimsdale, A. C.; Holmes, A. B. *Angew. Chem., Int. Ed.* **1998**, *37*, 402–428. (b) Mitschke, U.; Bäuerle, P. *J. Mater. Chem.* **2000**, *10*, 1471–1507. (c) Kulkarni, A. P.; Tonzola, C. J.; Babel, A.; Jenekhe, S. A. *Chem. Mater.* **2004**, *16*, 4556–4573. (d) Chen, C.-T. *Chem. Mater.* **2004**, *16*, 4389–4400. (e) D'Andrade, B. W.; Forrest, S. R. *Adv. Mater.* **2004**, *16*, 1585–1585. For recent contributions, see: (f) Huang, Q.; Evmenenko, G. A.; Dutta, P.; Lee, P.; Armstrong, N. R.; Marks, T. J. *J. Am. Chem. Soc.* **2005**, *127*, 10227–10242. (g) Kato, S. *J. Am. Chem. Soc.* **2005**, *127*, 11538–11539. (h) Yan, H.; Lee, P.; Armstrong, N. R.; Graham, A.; Evmenenko, G. A.; Dutta, P.; Marks, T. J. *J. Am. Chem. Soc.* **2005**, *127*, 3172–3183. (i) Wong, K.-T.; Chen, R.-T.; Fang, F.-C.; Wu, C.-C.; Lin, Y.-T. *Org. Lett.* **2005**, *7*, 1979–1982.

- (3) (a) Tang, C. W.; Vanslyke, S. A. *J. Appl. Phys.* **1987**, *51*, 913–915. (b) Tang, C. W.; Vanslyke, S. A.; Chen, C. H. *J. Appl. Phys.* **1989**, *65*, 3610–3616. (c) Burroughes, J. H.; Bradley, D. D. C.; Brown, A. R.; Marks, R. N.; Mackay, K.; Friends, R. H.; Burns, P. L.; Holmes, A. B. *Nature* **1990**, *347*, 539–541.



**Figure 1.** Organophosphorus moieties used to construct  $\pi$ -conjugated systems.

(Figure 1). However, before 2000 few oligomers<sup>6a</sup> and polymers<sup>6b</sup> featuring this P unit were known. In recent years, the family of phosphole-containing conjugated systems has been considerably extended with the synthesis of various mixed oligomers and polymers.<sup>7</sup> Moieties **B**,<sup>8a–c</sup> **C**,<sup>8d,e</sup> and **D**<sup>8f,g</sup> leading to P analogues of poly(aniline) and poly(para-phenylene-vinylene), respectively, have also been recently investigated.

The structural diversity of these building blocks illustrates the impact of phosphorus chemistry for the construction of conjugated macromolecules. Furthermore, one appealing property of these P building blocks is that they possess reactive phosphorus centers potentially allowing direct access to a range of novel  $\pi$ -conjugated systems. This possibility has been fully exploited for phosphole-based derivatives. We have shown that chemical modifications of the phosphorus atoms allow a fine-tuning of the optical and electrochemical properties of phosphole-based  $\pi$ -conjugated systems.<sup>7a–f</sup> In other words, starting from one phosphole-containing  $\pi$ -conjugated system, it is

**Table 1.** Photophysical Data for Benzophosphole Derivatives **2**, **3**, and **4**

	<b>1</b>	<b>2</b>	<b>3</b>	<b>4</b>		
	$T_{d10}^a$ (°C)	$\lambda_{max}^b$ (nm)	log $\epsilon$	$\lambda_{em}^b$ (nm)	$\phi_f^b$ (%)	$E_{p1/2}^c$ (eV)
<b>2</b>	213	332	2.9	366	4.2	−1.93
<b>3</b>	220	330	2.9	366	0.2	−1.92
<b>4</b>	220	333	3.0	366	13.4	−1.80 <sup>d</sup>

<sup>a</sup> TGA, 10% weight loss. <sup>b</sup> Measured in CH<sub>2</sub>Cl<sub>2</sub>, fluorescence quantum yield relative to quinine sulfate. <sup>c</sup> In CH<sub>2</sub>Cl<sub>2</sub>, referenced to SCE. <sup>d</sup>  $E_{pc}$ .

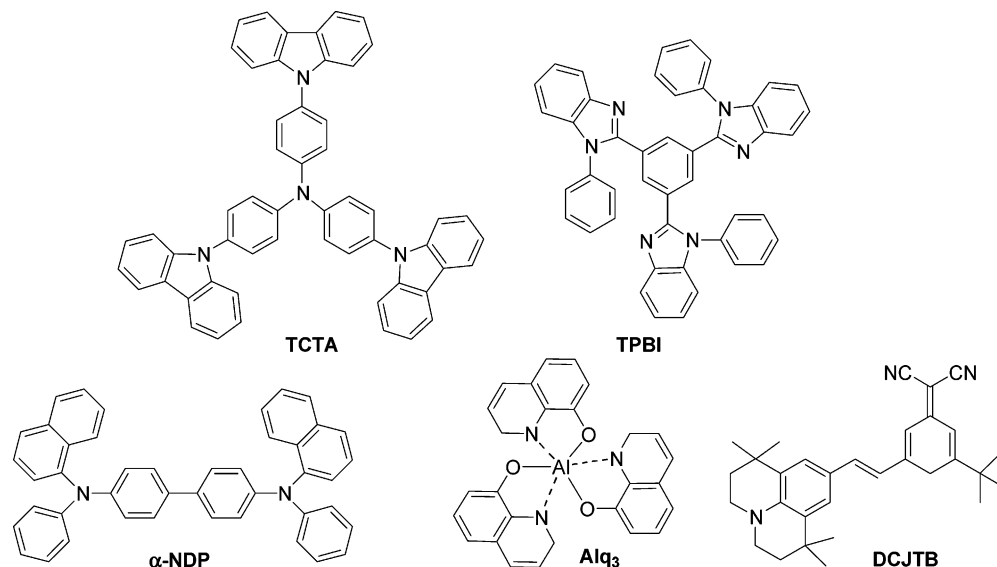
possible to readily access a family of derivatives with different physical characteristics. The next key challenge was to show that this unique possibility could be used to tailor conjugated materials for optoelectronic functions. For this purpose, we have selected OLEDs because this type of device demands multifunctional properties from a single organic material (thermal stability, luminescence efficiency, hole and electron injection, and transport capabilities...), which are difficult to optimize. In this paper, we report a full detailed study on the synthesis, use, and tailoring of phosphole-based oligomers and of their gold complexes as advanced materials for single- and multilayer OLEDs.<sup>9</sup> The conceptual design and specific properties that directly result from the presence of the P atom will be illustrated. We will show that exploiting the reactivity of the P atom is a key to tuning and to optimizing the material performances and also to avoiding or to inducing the aggregation of these P-chomophores in the solid state.

## Results and Discussion

**Physical Properties of Dibenzophosphole Derivatives.** We started this study using the long-standing and readily available dibenzophosphole derivatives **1–4** (Table 1),<sup>10</sup> although these derivatives do not display the usual properties of phospholes. In fact, due to their benzo-annulated structure, no significant interaction of the endocyclic  $\pi$ -system with the P moiety occurs and they behave as nonflexible arylphosphines.<sup>10</sup> For example, while pentasubstituted  $\sigma^3, \lambda^3$ -diarylphospholes are air-stable derivatives (vide infra),<sup>7</sup>  $\sigma^3, \lambda^3$ -dibenzophosphole **1** gives the corresponding oxide **2** upon exposure to air in the solid state. Its oxygen sensitivity precludes **1** from being used as a material for optoelectronic applications. Quite surprisingly, to the best of our knowledge, no physical data for compounds **2–4** are reported in the literature, although the optical properties of dibenzophosphole-aryl copolymers were recently described.<sup>11</sup> Derivatives **2–4** exhibit good thermal stabilities as estimated by thermogravimetric analysis (TGA) performed under nitrogen (Table 1). This parameter is important because low-molecular-weight species are deposited as thin films by vacuum evaporation for the fabrication of OLEDs. Furthermore, the thermal

- (4) (a) Yamagushi, S.; Tamao, K. *Chem. Lett.* **2005**, 34, 2–7. (b) Yamagushi, S.; Tamao, K. *J. Chem. Soc., Dalton Trans.* **1998**, 3693–3702. (c) Chan, L.-H.; Lee, R.-H.; Hsieh, C.-F.; Yeh, H.-C.; Chen, C.-T. *J. Am. Chem. Soc.* **2002**, 124, 6469–6479. (d) Yamagushi, S.; Endo, T.; Uchida, M.; Izumizawa, T.; Furukawa, K.; Tamao, K. *Eur. J. Chem.* **2000**, 6, 1683–1692. (e) Murata, H.; Kafafi, Z. H.; Uchida, M. *Appl. Phys. Lett.* **2002**, 80, 189–191. (f) Palilis, L. C.; Mäkinen, A. J.; Uchida, M.; Kafafi, Z. H. *Appl. Phys. Lett.* **2003**, 82, 2209–2211. (g) Kim, W.; Palilis, L. C.; Uchida, M.; Kafafi, Z. H. *Chem. Mater.* **2004**, 16, 4681–4686. (h) Liu, M. S.; Luo, J.; Jen, A. K.-Y. *Chem. Mater.* **2003**, 15, 3496–3500. (i) Yu, G.; Yin, Y.; Chen, J.; Xu, X.; Sun, X.; Ma, D.; Zhan, X.; Peng, Q.; Shui, Z.; Tang, B.; Zhu, D.; Fang, W.; Luo, Y. *J. Am. Chem. Soc.* **2005**, 127, 6335–6346. (j) Sohn, H.; Huddleston, R.; Power, D. R.; West, R. *J. Am. Chem. Soc.* **1999**, 121, 2935–2936. (k) Toal, S. J.; Jones, K. A.; Madge, D.; Trogler, W. C. *J. Am. Chem. Soc.* **2005**, 127, 11661–11665. (l) Zhen, L.; Dong, Y.; Mi, B.; Tang, Y.; Haeussler, M.; Tong, H.; Dong, Y.; Lam, J. W. Y.; Ren, Y.; Sung, H. H. Y.; Wong, K. S.; Ping, G.; Williams, I. D.; Kwok, H. S.; Tang, B. Z. *J. Phys. Chem. B* **2005**, 109, 10061–10066. (m) Uchida, M.; Izumizawa, T.; Nakano, T.; Yamagushi, S.; Tamao, K.; Furukawa, K. *Chem. Mater.* **2001**, 13, 2680–2683.
- (5) (a) Hissler, M.; Dyer, P.; Réau, R. *Coord. Chem. Rev.* **2003**, 244, 1–44. (b) Gate, D. *Top. Curr. Chem.* **2005**, 250, 107–126. (c) Hissler, M.; Dyer, P.; Réau, R. *Top. Curr. Chem.* **2005**, 250, 127–163. (d) Mathey, F. *Angew. Chem., Int. Ed.* **2003**, 42, 1578–1604.
- (6) (a) Deschamps, E.; Ricard, L.; Mathey, F. *Angew. Chem., Int. Ed. Engl.* **1994**, 11, 1158–1161. (b) Mathey, F.; Mercier, F.; Nief, F.; Fischer, J.; Mitschler, A. *J. Am. Chem. Soc.* **1982**, 104, 2077–2079. (c) Bevierre, O. M.; Mercier, F.; Ricard, L.; Mathey, F. *Angew. Chem., Int. Ed. Engl.* **1990**, 29, 655–657. (d) Deschamps, E.; Ricard, L.; Mathey, F. *Heteroat. Chem.* **1991**, 2, 377–383. (e) Mao, S. S. H.; Don Tilley, T. *Macromolecules* **1997**, 30, 5566–5569.
- (7) (a) Hay, C.; Le Vilain, D.; Deborde, V.; Toupet, L.; Réau, R. *Chem. Commun.* **1999**, 345–346. (b) Hay, C.; Fischmeister, C.; Hissler, M.; Toupet, L.; Réau, R. *Angew. Chem., Int. Ed.* **2000**, 10, 1812–1815. (c) Hay, C.; Hissler, M.; Fischmeister, C.; Rault-Berthelot, J.; Toupet, L.; Nyulaszi, L.; Réau, R. *Chem.-Eur. J.* **2001**, 7, 4222–4236. (d) Fave, C.; Hissler, M.; Sénéchal, K.; Ledoux, I.; Zyss, J.; Réau, R. *Chem. Commun.* **2002**, 1674–1675. (e) Hay, C.; Fave, C.; Hissler, M.; Rault-Berthelot, J.; Réau, R. *Org. Lett.* **2003**, 19, 3467–3470. (f) Fave, C.; Hissler, M.; Karpati, T.; Rault-Berthelot, J.; Deborde, V.; Toupet, L.; Nyulaszi, L.; Réau, R. *J. Am. Chem. Soc.* **2004**, 136, 6058–6063. (g) Morisaki, Y.; Aiki, Y.; Chujo, Y. *Macromolecules* **2003**, 36, 2594–2597. (h) Baumgartner, T.; Neumann, T.; Wirges, B. *Angew. Chem., Int. Ed.* **2004**, 43, 6197–6201. (i) Baumgartner, T.; Bergmans, W.; Karpati, T.; Neumann, T.; Nieger, M.; Nyulaszi, L. *Chem.-Eur. J.* **2005**, 11, 4687–4699. (j) Makioka, M.; Hayashi, T.; Tanaka, M. *Chem. Lett.* **2004**, 33, 44–45. (k) Niemi, T. A.; Coe, P. L.; Till, S. J. *J. Chem. Soc., Perkin Trans.* **2000**, 1, 1519.
- (8) (a) Lucht, B. L.; St. Onge, N. O. *Chem. Commun.* **2000**, 2097–2099. (b) Jin, Z.; Lucht, B. L. *J. Organomet. Chem.* **2002**, 653, 167–176. (c) Jin, Z.; Lucht, B. L. *J. Am. Chem. Soc.* **2005**, 127, 5586–5595. (d) Wright, V. A.; Gates, D. P. *Angew. Chem., Int. Ed.* **2002**, 41, 2389–2392. (e) Smith, R. C.; Chen, X.; Protasiewicz, J. D. *Inorg. Chem.* **2003**, 42, 5468–5470. (f) Smith, R. C.; Protasiewicz, J. D. *J. Am. Chem. Soc.* **2004**, 126, 2268–2269. (g) Cosmina, D.; Shashin, S.; Smith, R. C.; Choua, S.; Berclaz, T.; Geoffroy, M.; Protasiewicz, J. D. *Inorg. Chem.* **2003**, 42, 6241–6251.

- (9) For a preliminary communication, see: Fave, C.; Cho, T.-Y.; Hissler, M.; Chen, C.-W.; Luh, T.-Y.; Wu, C.-C.; Réau, R. *J. Am. Chem. Soc.* **2003**, 125, 9254–9255.
- (10) (a) Quin, L. D.; Quin, G. S. In *Phosphorus–Carbon Heterocyclic Chemistry: The Rise of a New Domain*; Mathey, F., Ed.; Elsevier Science Ltd: Oxford, 2001. (b) Mathey, F. *Chem. Rev.* **1988**, 88, 429–453. (c) Attar, S.; Bearden, W. H.; Alcock, N. W.; Aleya, E. C.; Nelson, J. H. *Inorg. Chem.* **1990**, 29, 425–433. (d) Egan, W.; Tang, R.; Zon, G.; Mislow, K. *J. Am. Chem. Soc.* **1971**, 93, 6205–6216.
- (11) Kobayashi, S.; Noguchi, M.; Tsubata, Y.; Kitano, M.; Doi, H.; Kamioka, T.; Nakazono, A. Japanese Patent 2003231741, 2003.



**Figure 2.** Structures of multilayer OLED constituent materials: TCTA (HTM), TPBI (ETM), α-NPD (HTM), Alq<sub>3</sub> (ETM), and DCJTb (dopant).

instability of organic materials is considered to be a major cause of the poor high-temperature operating stability of OLEDs.<sup>2,12</sup> Cyclic voltammetry (CV) performed at 200 mV s<sup>-1</sup> in CH<sub>2</sub>Cl<sub>2</sub> solution revealed reduction processes occurring at similar potentials for the three compounds (Table 1). The reduction processes are reversible for compounds **2** and **3** and irreversible for the gold complex **4**. No oxidation peak was observed under these experimental conditions. The UV-vis spectra of dibenzophospholes **2–4** are similar; they show weak absorptions around 330 nm (Table 1). These absorptions in the UV region reveal that these derivatives possess large “optical” HOMO–LUMO gaps, as observed for structurally related fluorenes<sup>13</sup> and fused dithienophospholes.<sup>7h,i</sup> This feature is in accordance with the view that dibenzophospholes have to be considered as P-bridged biphenyl derivatives. The three dibenzophosphole derivatives **2–4** are photoluminescent and emit in the UV region at similar wavelengths (Table 1). Note that the Stokes shifts are relatively small (ca. 32–36 nm), suggesting minimal rearrangement of these rigid molecules upon photoexcitation. The quantum yields depend on the nature of the P-modification, the gold(I) complex **4** exhibiting the highest value in solution (Table 1). In marked contrast, in the solid state only photoluminescence (PL) from the oxodibenzophosphole **2** can be detected ( $\lambda_{\text{em}} = 370$  nm). This result prompted us to investigate only this compound as a material for the fabrication of OLEDs.

**OLEDs Incorporating Dibenzophosphole Derivatives.** The devices employed in this study have the typical structure of organic layers sandwiched between the bilayer anode [indium–tin oxide/poly(3,4-ethylenedioxythiophene)-polystyrenesulfonate, ITO/PEDOT-PSS] and the cathode. The low-molecular-weight

organic layers were deposited by thermal evaporation under high vacuum.<sup>14</sup> The configuration of the single-layer OLEDs is ITO/PEDOT:PSS(25 nm)/organic layer(100 nm)/Mg:Ag(80 nm)/Ag(150 nm). Using **2** as the organic layer, light emission was observed for a turn-on voltage of 4 V. However, the device is unstable and its electroluminescence characteristics (emission wavelength, brightness...) vary rapidly with applied driving current. Derivative **2** was also tested in two-layer OLEDs having the configuration of ITO/PEDOT/TCTA/2/Mg:Ag/Ag and ITO/PEDOT/2/TPBI/Mg:Ag/Ag, respectively. In the former heterostructure device, **2** is used in combination with the known large-gap hole-transport material (HTM) TCTA (Figure 2), to check whether **2** can serve as an electron-transport and emitting layer, while in the latter device, **2** is used in combination with the known large-gap electron-transport material (ETM) TPBI (Figure 2), to test whether **2** can serve as a hole-transport and emitting layer. Here also, the device characteristics changed rapidly with applied driving current. These results show that dibenzophospholes are not suitable derivatives for the construction of OLEDs and prompted us to study another series of P-containing oligomers incorporating phosphole units.

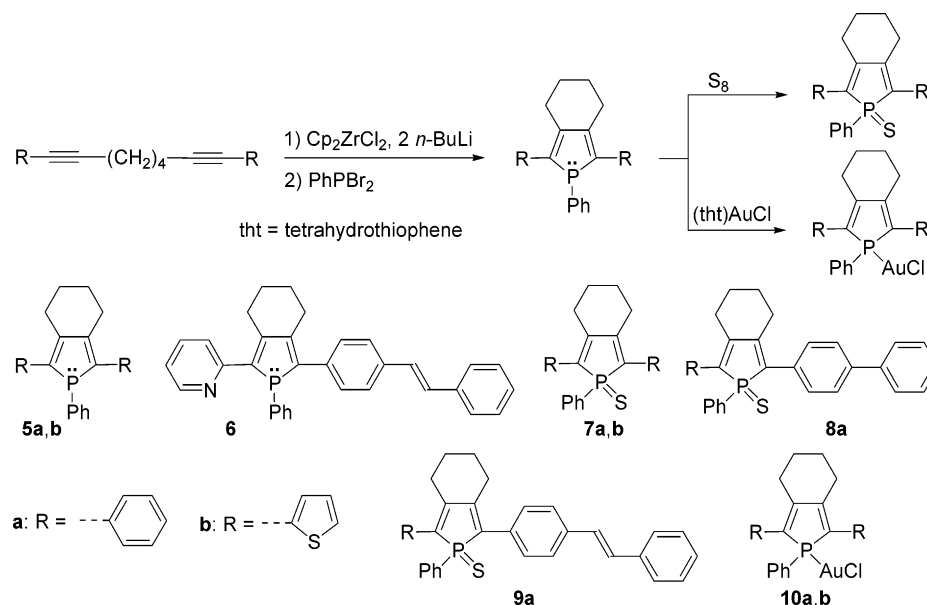
**Synthesis and Physical Properties of Phosphole Derivatives.** Phospholes are interesting building blocks for the tailoring of  $\pi$ -conjugated oligomers because they possess properties that are markedly different from those of thiophenes and pyrroles.<sup>5,10</sup> The tricoordinate phosphorus atom of phospholes has a pyramidal geometry with a lone pair having pronounced s-character. These geometric and electronic features prevent an efficient endocyclic conjugation of the electron sextet, and, as a consequence, the phosphole ring exhibits a low aromatic character and a reactive heteroatom.<sup>10a,b,15</sup> These properties are of particular interest for the construction of  $\pi$ -conjugated systems with low HOMO–LUMO separation<sup>7</sup> because conjugation

(12) Tokito, S.; Tanaka, H.; Noda, K.; Okada, A.; Taga, Y. *Appl. Phys. Lett.* **1997**, *70*, 1929–1931.

(13) (a) Su, H.-J. S.; Wu, F.-I.; Shu, C.-F. *Macromolecules* **2004**, *37*, 7197–7202. (b) Setayesh, S.; Grimsdale, A. C.; Weil, T.; Enkelmann, V.; Mullen, K.; Meghdadi, F.; List, E. J. W.; Leising, G. *J. Am. Chem. Soc.* **2001**, *123*, 946–953. (c) Marsitzky, D.; Vestberg, R.; Blainey, P.; Tang, B. T.; Hawker, C. J. *J. Am. Chem. Soc.* **2001**, *123*, 6965–6972. (d) Klärner, G.; Müller, R. D. *Macromolecules* **1998**, *31*, 2007–2009. (e) Marsitzky, D.; Klapper, M.; Müller, K. *Macromolecules* **1999**, *32*, 8685–8688. (f) Pei, Q.; Yang, Y. *J. Am. Chem. Soc.* **1996**, *118*, 7416–7417. (g) Ego, C.; Grimsdale, A. C.; Uckert, F.; Yu, G.; Srdanov, G.; Mullen, K. *Adv. Mater.* **2002**, *14*, 809–811. (h) Wu, F.-I.; Reddy, D. S.; Shu, C.-F.; Liu, M. S.; Jen, A. K.-Y. *Chem. Mater.* **2003**, *15*, 269–274. (i) Shu, C.-F.; Dodda, R.; Wu, F.-I.; Liu, M. S.; Jen, A. K.-Y. *Macromolecules* **2003**, *36*, 6698–6703.

(14) Wu, C.-C.; Chen, C.-W.; Lin, Y.-T.; Yu, H.-L.; Hsu, J.-H.; Luh, T.-Y. *Appl. Phys. Lett.* **2001**, *79*, 3023–3025.

(15) (a) Nyulaszi, L. *Chem. Rev.* **2001**, *101*, 1229–1246. (b) Mattmann, E.; Mathey, F.; Sevin, A.; Frisson, G. *J. Org. Chem.* **2002**, *67*, 1208–1213. (c) Delaere, D.; Dransfeld, A.; Nguyen, M. T.; Vanquickenborne, L. G. *J. Org. Chem.* **2000**, *65*, 2631–2636. (d) Delaere, D.; Nguyen, M. T.; Vanquickenborne, L. G. *Phys. Chem. Chem. Phys.* **2002**, *4*, 1522–1530. (e) Salznier, U.; Lagowski, J. B.; Pickup, P. G.; Poirier, R. A. *Synth. Met.* **1998**, *96*, 177–189. (f) Ma, J.; Li, S.; Jiang, Y. *Macromolecules* **2002**, *35*, 1109–1115.

**Scheme 1.** General Synthetic Route to 2,5-Diarylphospholes, Their Thiooxo Derivatives, and Gold Complexes, and Structures of the Studied P Compounds**Table 2.** Photophysical and Electrochemical Data for Derivatives **6**, **7a,b**, **8a**, **9a**, and **10a,b**

	Td <sub>10</sub> <sup>a</sup> (°C)	λ <sub>max</sub> <sup>b</sup> (nm)	log ε	λ <sub>em</sub> <sup>b</sup> (nm)	φ <sub>f</sub> <sup>c</sup> (%)	τ <sup>b</sup> (ns)	λ <sub>max</sub> <sup>d</sup> (nm)	λ <sub>em</sub> <sup>d</sup> (nm)	φ <sub>f</sub> <sup>e</sup> (%)	τ <sup>d</sup> (ns)	E <sub>pc</sub> <sup>f</sup> (eV)	E <sub>pa</sub> <sup>f</sup> (eV)
<b>6</b>	306	395	4.36	497	15.2	0.92	410	520	3.6	0.30	−1.95	+1.04
<b>7a</b>	210	380	4.13	516	0.05 <sup>g</sup>	0.025	345	517	0.5	0.38	−1.74	+1.52
<b>7b</b>	253	432	3.98	548	4.6	0.41	435	553	6.6	1.33	−1.55	+1.08
<b>8a</b>	287	396	3.90	527	0.37	0.024	397	526	0.8	0.38	−1.70	+1.45
<b>9a</b>	252	412	3.44	542	2.0	0.16	410	545	4.2	0.52	−1.68	+1.31
<b>10a</b>	251	358	3.80	506	7.3	0.52	360	505/630	11.2	0.94/5.20	−1.75	+1.85
<b>10b</b>	218	428	4.10	544	12.9	1.83	440	550/690	0.6	0.25/1.54	−1.35	+1.22

<sup>a</sup> TGA, 10% weight loss. <sup>b</sup> In CH<sub>2</sub>Cl<sub>2</sub>. <sup>c</sup> Absolute fluorescence quantum yield in CH<sub>2</sub>Cl<sub>2</sub>. <sup>d</sup> In neat film. <sup>e</sup> Absolute fluorescence quantum yield in neat film. <sup>f</sup> In CH<sub>2</sub>Cl<sub>2</sub>, referenced to SCE. <sup>g</sup> The QY is too low to be measured upon excitation at 442 nm with HeCd Laser; this value was obtained in CH<sub>2</sub>Cl<sub>2</sub> solution relative to quinine sulfate.

tion is enhanced for macromolecules composed of units exhibiting low resonance energies.<sup>1e,15c–f</sup> However, the most appealing property of the phosphole ring for tailoring molecular materials is the possibility of fine-tuning the physical characteristics (redox potentials, absorption and emission wavelengths...) of phosphole-containing conjugated systems by simple chemical modification (oxidation, complexation...) of the P centers.<sup>5,7</sup> Note that the tuning of the electron affinity (EA) and ionization potential (IP) is of great interest to optimize the energy differences between the LUMO and HOMO levels and work functions of cathodes and anodes, respectively, to favor hole and electron injection into OLEDs.

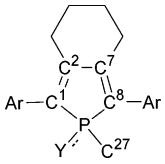
The first property to be considered is the thermal stability of phosphole-based oligomers, because the OLED fabrication process involves thermal evaporation of these low-molecular-weight oligomers. Derivatives **5a,b** (Scheme 1) featuring σ<sup>3</sup>,λ<sup>3</sup>-phosphole rings possess rather low decomposition temperatures,<sup>7c</sup> which preclude their deposition by vacuum sublimation. It is likely that the thermal instability of derivatives **5a,b** is due to the isomerization of these 1*H*-phospholes into 2*H*-phospholes, which are extremely reactive species.<sup>16</sup> Two strategies were investigated to overcome the thermal instability of σ<sup>3</sup>,λ<sup>3</sup>-phospholes. The first approach, which is a “trial and error” one,

consists of varying the ring substituents at the 2,5-positions. A systematic study involving the synthesis of compounds bearing substituted phenyl, thienyl, and pyridyl moieties revealed that the mixed σ<sup>3</sup>-derivative **6** (Scheme 1) has a high decomposition temperature (306 °C). The second approach involves the chemical modification of the P atom, because it is known that the 1*H*-phosphole → 2*H*-phosphole isomerization process is less favored for σ<sup>4</sup>-phospholes.<sup>16b</sup> Indeed, the decomposition temperatures of σ<sup>4</sup>-thiooxophospholes **7a** and **7b** (Scheme 1) are increased by 86 and 48 °C, respectively, in comparison to their σ<sup>3</sup>-phosphole precursors **5a** and **5b**. These results prompted us to varying the substitution pattern of σ<sup>4</sup>-thiooxophospholes to extend the family of these thermally stable compounds. The molecular design for the new σ<sup>4</sup>-thiooxo(2-phenyl)phospholes relies on the introduction of 4-biphenyl or 4-stilbenyl substituents at the 5-position of the P-ring with the view to vary the conjugated path. Indeed, these compounds **8a** and **9a** (Scheme 1) also have rather high decomposition temperatures as estimated by TGA (Table 2). The synthetic route to the newly synthesized derivatives employs the one-pot “Fagan–Nugent method”<sup>17</sup> involving the oxidative coupling of functionalized octa-1,7-diyne with zirconocene followed by treatment with PhPBr<sub>2</sub>

- (17) (a) Fagan, P. J.; Nugent, W. A. *J. Am. Chem. Soc.* **1988**, *110*, 2310–2312. (b) Fagan, P. J.; Nugent, W. A.; Calabrese, J. C. *J. Am. Chem. Soc.* **1994**, *116*, 1880–1889. (c) Sava, X.; Mézaille, N.; Maigrot, N.; Nief, F.; Ricard, L.; Mathey, F.; Le Floch, P. *Organometallics* **1999**, *18*, 4205–4215. (d) Negishi, E.; Takahashi, T. *Acc. Chem. Res.* **1994**, *27*, 124–130.

(16) (a) Mathey, F. *Acc. Chem. Res.* **2004**, *37*, 954–960. (b) Charrier, C.; Bonnard, H.; De Lauzon, G.; Mathey, F. *J. Am. Chem. Soc.* **1983**, *105*, 6871–6877.



**Table 3.** Selected Bond Lengths [Å] and Twist Angles between the Phosphole Ring and Its 2- and 5-Substituents [deg] for Thiooxophospholes **7a**, **8a**, and **9a** (Y = S) and Complexes **10a,b** (Y = Au–Cl)


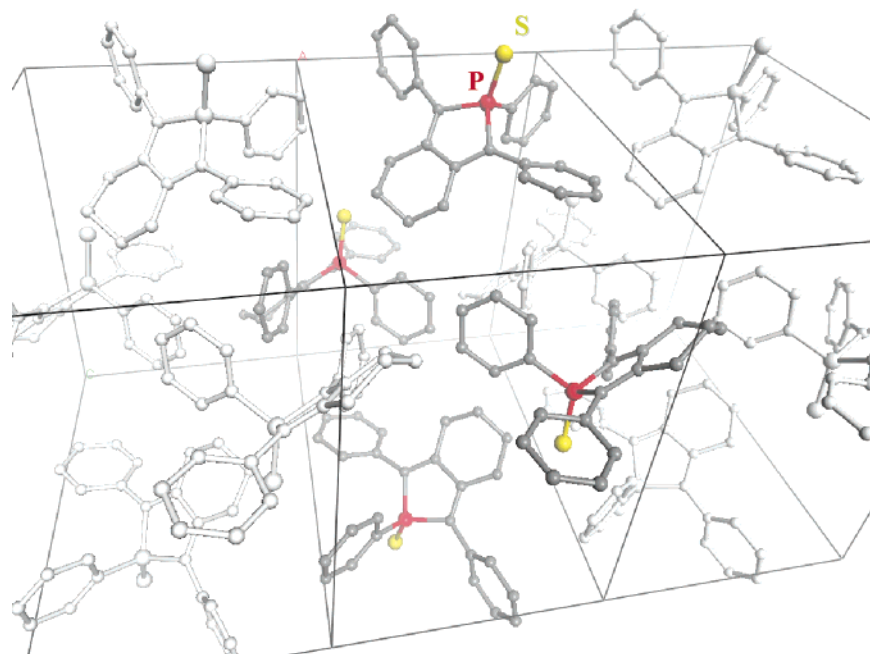
	<b>7a</b> (Y = S)	<b>8a</b> (Y = S)	<b>9a</b> (Y = S)	<b>10a</b> (Y = AuCl)	<b>10b</b> (Y = AuCl)
P–C(1)	1.816(2)	1.809(2)	1.812(2)	1.801(6)	1.817(6)
C(1)–C(2)	1.346(3)	1.364(3)	1.351(3)	1.350(9)	1.358(9)
C(2)–C(7)	1.493(3)	1.489(3)	1.494(3)	1.484(9)	1.483(9)
C(7)–C(8)	1.345(3)	1.354(3)	1.353(3)	1.346(9)	1.359(6)
C(8)–P	1.806(2)	1.809(2)	1.8109(18)	1.802(6)	1.806(3)
P–Au				2.229(1)	2.2300(16)
Au–Cl				2.284(1)	2.2895(19)
C(1)–P–C(8)	93.38(8)	93.67(11)	92.97(8)	93.3(3)	93.2(3)
C(1)–P–C(27)	105.09(8)	102.71(10)	106.17(8)	110.4(3)	105.0(3)
C(1)–P–Y	119.54(6)	119.13(8)	118.24(7)	114.4(2)	121.30(18)
C(8)–P–C(27)	107.95(8)	110.21(10)	111.87(9)	105.8(3)	107.3(3)
C(8)–P–Y	115.27(6)	116.31(8)	112.78(6)	116.7(2)	116.48(19)
C(27)–P–Y	113.40(6)	112.70(8)	113.12(7)	114.2(2)	111.48(19)
P–Au–Cl				177.64(7)	174.63(8)
twist angles	50.3/50.5	36.3/35.9	47.2/44.6	47.3/54.7	3.8/13.0

**Table 4.** Crystallographic Data and Structural Refinement Details for **7a**, **8a**, **9a**, **10a**, and **10b**

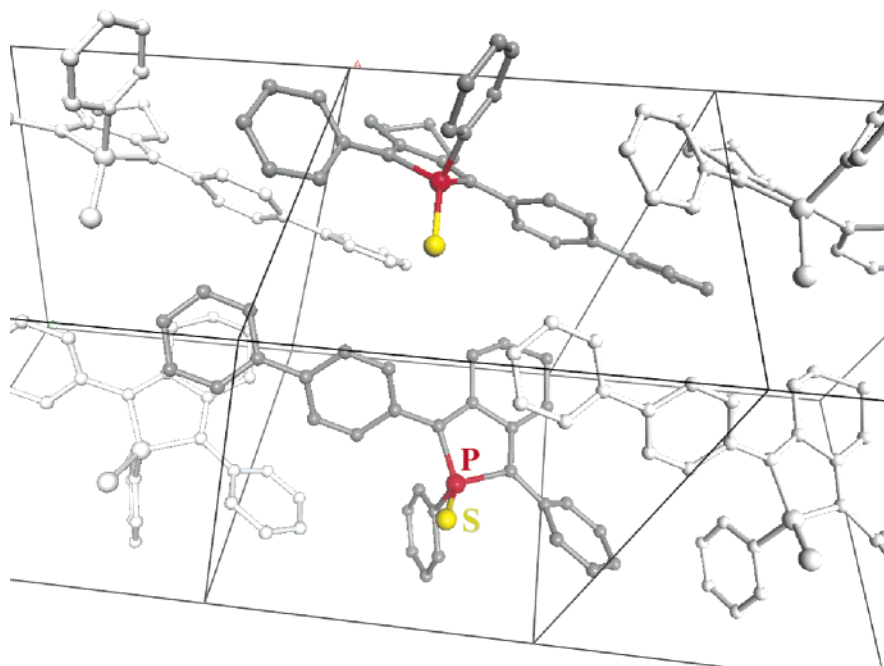
	<b>7a</b>	<b>8a</b>	<b>9a</b>	<b>10a</b>	<b>10b</b>
molecular formula	C <sub>26</sub> H <sub>23</sub> PS	C <sub>32</sub> H <sub>27</sub> PS	C <sub>34</sub> H <sub>29</sub> PS	C <sub>26</sub> H <sub>23</sub> AuClP	C <sub>22</sub> H <sub>19</sub> AuClPS <sub>2</sub>
molecular weight, g/mol	398.47	474.57	500.60	641.29	610.88
<i>a</i> , Å	9.634(5)	9.907(5)	9.256(5)	10.377(5)	9.0350(10)
<i>b</i> , Å	15.725(5)	10.282(5)	12.399(5)	17.347(5)	9.542(3)
<i>c</i> , Å	14.360(5)	12.655(5)	13.325(5)	13.471(5)	14.598(2)
$\alpha$ , deg	90	90	95.791(5)	90	71.62(2)
$\beta$ , deg	93.621(5)	105.568(5)	109.093(5)	91.769(5)	78.250(10)
$\gamma$ , deg	90	90	108.521(5)	90	63.25(2)
<i>V</i> , Å <sup>3</sup>	2171.1(15)	1241.8(10)	1334.0(10)	2423.8(16)	1063.7(4)
<i>Z</i>	4	2	2	4	2
<i>D</i> <sub>calc</sub> , g cm <sup>−3</sup>	1.219	1.269	1.246	1.757	1.907
crystal system	monoclinic	monoclinic	triclinic	monoclinic	triclinic
space group	<i>P</i> 2 <sub>1</sub> / <i>n</i>	<i>P</i> 2 <sub>1</sub>	<i>P</i> -1	<i>P</i> 2 <sub>1</sub> / <i>n</i>	<i>P</i> -1
<i>T</i> , K	293(2)	293(2)	293(2)	293(2)	293(2)
wavelength Mo K $\alpha$ , Å	0.71069	0.71069	0.71069	0.71069	0.71069
$\mu$ , mm <sup>−1</sup>	0.231	0.214	0.203	6.368	0.732
<i>F</i> (000)	840	500	528	1244	588
$\theta$ limit, deg	2.93–27.54	2.33–27.12	3.27–27.49	2.44–30.03	1.47–26.94
no. reflns collected	9750	5273	10 446	12 868	4887
no. ind reflns	4985	5273	6083	7066	4593
reflections [ <i>I</i> > 2 $\sigma$ ( <i>I</i> )]	3877	4735	4163	5271	3785
data/restraints/parameters	4985/0/254	5273/1/308	60 837/0/326	7066/0/285	4593/0/245
GOF on <i>F</i> <sup>2</sup>	1.052	1.077	1.025	1.032	1.075
final <i>R</i> indices	<i>R</i> 1 = 0.0456	<i>R</i> 1 = 0.0424	<i>R</i> 1 = 0.0467	<i>R</i> 1 = 0.0461	<i>R</i> 1 = 0.0356
[ <i>I</i> > 2 $\sigma$ ( <i>I</i> )]	<i>wR</i> 2 = 0.1231	<i>wR</i> 2 = 0.1092	<i>wR</i> 2 = 0.1158	<i>wR</i> 2 = 0.1074	<i>wR</i> 2 = 0.0914
<i>R</i> indices (all data)	<i>R</i> 1 = 0.0616	<i>R</i> 1 = 0.0495	<i>R</i> 1 = 0.0783	<i>R</i> 1 = 0.0701	<i>R</i> 1 = 0.0541
	<i>wR</i> 2 = 0.1361	<i>wR</i> 2 = 0.1165	<i>wR</i> 2 = 0.1334	<i>wR</i> 2 = 0.1189	<i>wR</i> 2 = 0.0972
largest diff peak and hole (e Å <sup>−3</sup> )	0.241 and −0.298	0.311 and −0.316	0.381 and −0.267	1.483 and −1.428	1.187 and −1.148

(Scheme 1). It is worth noting that this synthetic pathway is rather simple and efficient, allowing gram-scale preparations, because the functionalized octa-1,7-diynes are obtained in good yields by Sonogashira couplings. The thiooxophospholes are readily prepared by treatment of the corresponding phosphole with elemental sulfur (Scheme 1). Derivatives **6** and **7a–9a** are air-stable compounds that can be easily purified by column chromatography. They are readily soluble in common organic solvents such as CH<sub>2</sub>Cl<sub>2</sub>, THF, or CH<sub>3</sub>CN. They exhibit classical NMR data, and their structures were supported by high-resolution mass spectrometry and elemental analysis.  $\sigma^4$ -Thiooxophospholes **8a** and **9a**, as well as the related 2,5-

diphenylphosphole **7a**, were subjected to X-ray diffraction study to elucidate their molecular structures and bulk molecular-packing characteristics (Tables 3 and 4, Figures 3–5). The bond lengths and valence angles of the P-ring of **8a** and **9a** are typical<sup>7c</sup> and compare with those of **7a** (Table 3). In these three compounds, the P atom exhibits a distorted tetrahedral geometry (Figures 3–5) due to the small endocyclic C(1)–P–C(8) angles [**7a**, 93.38°(8); **8a**, 93.67°(11); **9a**, 92.97°(8)]. Of particular interest, these crystal structures show that the diarylphospholyl moieties do not have a planar conformation. The rotational disorder depends on the substitution pattern of the  $\sigma^4$ -thiooxophospholes. The twist angles between the phosphole ring and



**Figure 3.** Perspective view of the packing of 2,5-diphenylthioxophosphole **7a** in crystalline phase. H atoms are omitted for clarity.

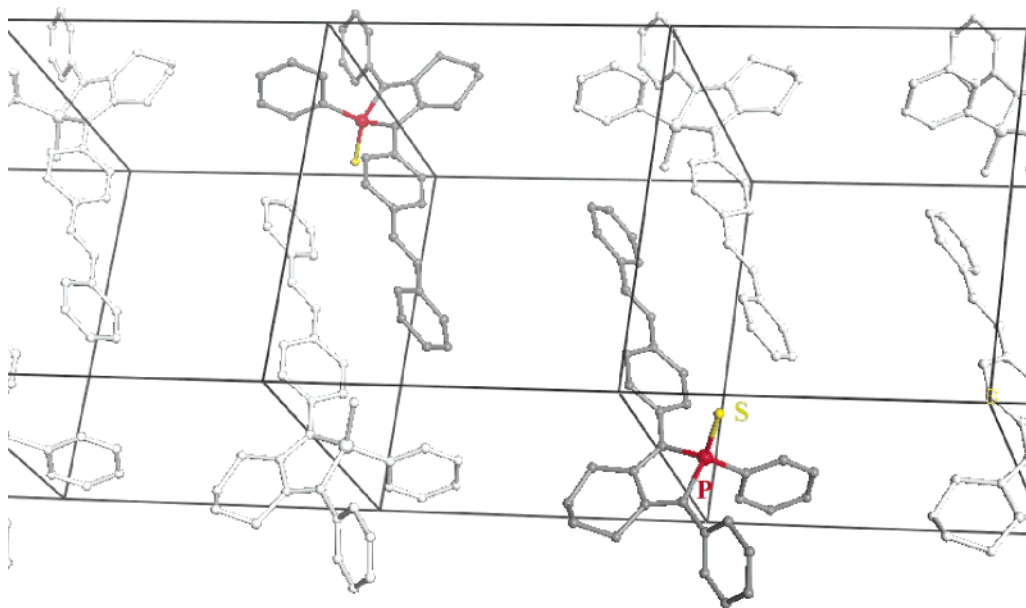


**Figure 4.** Perspective view of the packing of 2-phenyl-5-biphenylthioxophosphole **8a** in crystalline phase. H atoms are omitted for clarity.

the aromatic substituents are similar for 2,5-diphenylphosphole **7a** (50.3° and 50.5°) and 2-phenyl-stilbenylphosphole **9a** (44.6° and 47.2°), but much smaller for 2-biphenyl-5-phenylphosphole **8a** (35.9° and 36.3°). The lower rotational disorder observed for derivative **8a** should favor the delocalization of the  $\pi$ -system because the orbital overlap varies approximately with the cosine of the twist angle. This is supported by the fact that the inter-ring phosphole–phenyl distances are slightly smaller for derivative **8a** [1.470(3)–1.473(3) Å] than for the highly rotationally disordered compounds **7a** [1.479(2)–1.480(2) Å] and **9a** [1.479(2)–1.481(2) Å]. Note that the twist angle (23.0°) and the inter-ring distance [1.484(3) Å] of the biphenyl moiety of **8a** are classical and that the stilbenyl fragment of **9a** is almost planar. The above results indicate that  $\sigma^4$ -thioxophospholes

have a three-dimensional nonplanar molecular structure. These structural features are of particular interest because they could reduce the intermolecular interaction and the likelihood of excimer formation in solid films (vide infra).

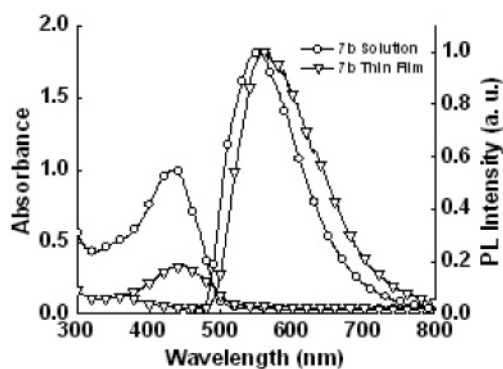
The photophysical and electrochemical properties of these derivatives are presented in Table 2. The published optical data for **7a,b**<sup>7b</sup> have been completed by lifetime measurements of excited states and studies of thin films deposited by vacuum sublimation. It is noteworthy that 2,5-diphenylthioxophosphole **7a** exhibits properties that are significantly different from those of the corresponding dibenzophosphole **3**. The Stokes shift of the less rigid compound **7a** is much higher than that of **3** (**7a**, 167 nm; **3**, 36 nm), and thioxophosphole **7a** is more easily reduced and oxidized than **3** (Tables 1 and 2). These physical



**Figure 5.** Perspective view of the packing of 2-phenyl-5-stilbenylthioxophosphole **9a** in crystalline phase. H atoms are omitted for clarity.

data nicely illustrate the profound difference in electronic structures between 2,5-diarylphospholes and dibenzophospholes.

All phosphole derivatives exhibit an intense band in the UV–visible region attributed to the  $\pi$ – $\pi^*$  transitions of the conjugated system. Upon increasing the length of the conjugated path of  $\sigma^4$ -thioxophospholes (**7a/8a/9a**, Scheme 1), the  $\lambda_{\text{max}}$  is red-shifted, indicating a decrease in the optical HOMO–LUMO energy separations (Table 2). Only a single emission peak was observed for the three compounds with Stokes shifts ranging from 75 to 165 nm (Table 2). The lifetimes ( $\tau$ ) of excited  $\sigma^3$ - and  $\sigma^4$ -phosphole derivatives are in the nanosecond range, suggesting fluorescence processes involving emission from singlet excited states (Table 2). The absolute quantum yields in solution measured with a calibrated integrating sphere system<sup>18</sup> are rather modest and depend on the structure of the phospholes (Table 2), the most efficient fluorophore being the  $\sigma^3$ -phosphole **6** ( $\phi_f = 15.2\%$ ). This behavior is remarkable because chromophores featuring  $\sigma^3$ -P centers usually exhibit almost no fluorescence as a result of quenching by the P lone pair.<sup>19</sup> This result nicely illustrates the unique properties of phospholes as compared to usual phosphines. It is interesting to note that, while the absolute quantum yield of **6** decreases in the solid state ( $\phi_f = 3.6\%$ ), the quantum yields<sup>18</sup> for all  $\sigma^4$ -thioxophospholes are higher in the solid state than in dilute solution (Table 2). This behavior is surprising because photoluminescent organic chromophores are usually less emissive in the solid state than in solution due to molecular aggregation forming less emissive species such as excimers.<sup>20</sup> It is likely that this rather unusual behavior is due to the steric protection provided by the substituents (Ph, S) of the tetrahedral P atom

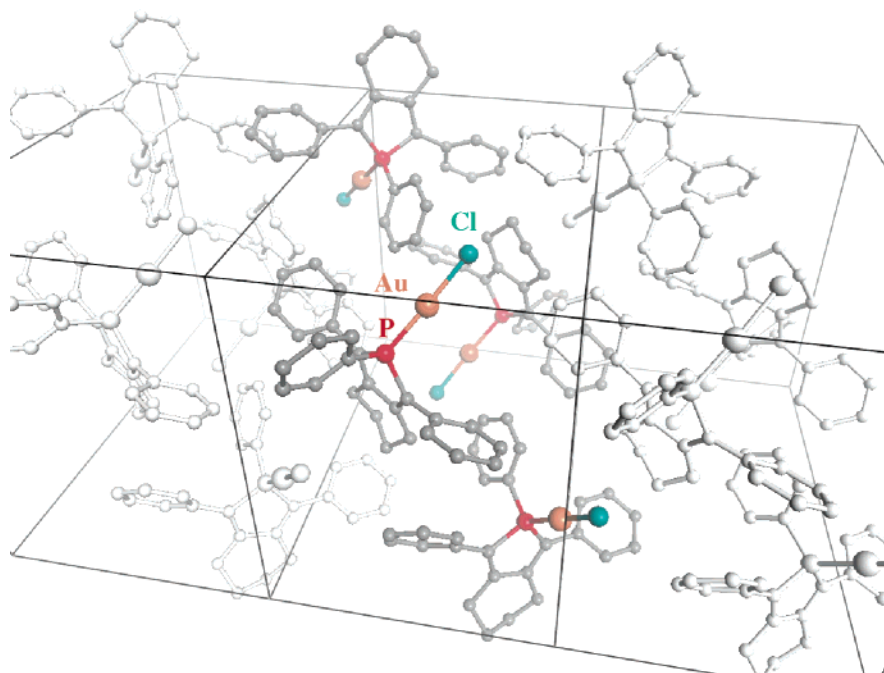


**Figure 6.** UV–vis and fluorescence spectra of **7b** in  $\text{CH}_2\text{Cl}_2$  solution and in thin film.

and the nonplanarity of the diarylphosphole moiety, which preclude a close cofacial organization of these P chromophores in the solid state. This hypothesis is supported by two facts. First, the UV–vis and fluorescence spectra of  $\sigma^4$ -thioxophospholes in solution and in thin film are similar (Table 2); no red-shifted emission revealing excimer or aggregate formation is observed (Figure 6). Second, although care must be taken when comparing different states of matter (amorphous vs crystalline, vide infra), the packing of  $\sigma^4$ -thioxophospholes **7a**, **8a**, and **9a** in monocrystals clearly shows the site isolation of these P chromophores (Figures 3–5). The steric protection provided by the substituents of the tetrahedral P atoms can be seen plainly in these figures. Such rare enhancement of fluorescence in the solid state was also reported for phenyl-substituted siloles<sup>20a–d</sup> and is attributed to a restriction in the solid state of the rotation of the 2,5-phenyl substituents, which

- (18) (a) Wu, C.-C.; Hung, W.-Y.; Liu, T.-L.; Zhang, L.-Z.; Luh, T.-Y. *J. Appl. Phys.* **2003**, *93*, 5465–5471. (b) Chao, T.-C.; Lin, Y.-T.; Chang, C.-Y.; Hung, T.-S.; Chou, H.-C.; Wu, C.-C.; Wong, K.-T. *Adv. Mater.* **2005**, *17*, 992–996.
- (19) (a) Yamaguchi, S.; Akiyama, S.; Tamao, K. *J. Organomet. Chem.* **2002**, *646*, 277–281. (b) Wang, Y.; Ranasinghe, M. I.; Goodson, T. *J. Am. Chem. Soc.* **2003**, *125*, 9562–9563. (c) Smith, R. C.; Protasiewicz, J. D. *J. Chem. Soc., Dalton Trans.* **2000**, 4738–4741. (d) Smith, R. C.; Earl, M. J.; Protasiewicz, J. D. *Inorg. Chem. Acta* **2004**, *357*, 4139–4143. (e) Kang, Y.; Song, D.; Schmäder, H.; Wang, S. *Organometallics* **2002**, *21*, 2413–2421.

- (20) (a) Luo, J.; Xie, Z.; Lam, J. W. Y.; Cheng, L.; Chen, H.; Qui, C.; Kwok, H. S.; Zhan, X.; Liu, Y.; Zhu, D.; Tang, B. Z. *Chem. Commun.* **2001**, 1740–1741. (b) Chen, J.; Xie, Z.; Lam, J. W. Y.; Tang, B. Z. *Macromolecules* **2003**, *36*, 1108–1117. (c) Ren, Y.; Lam, J. W. Y.; Dong, Y.; Tang, B. Z.; Wong, K. S. *J. Phys. Chem.* **2005**, *109*, 1135–1140. (d) Chen, J.; Xu, B.; Cao, Y.; Sung, H. H. Y.; Williams, I. D.; Tang, B. Z. *J. Phys. Chem.* **2005**, *109*, 17086–17093. (e) Levitus, M.; Schmieder, K.; Ricks, H.; Shimizu, K. D.; Bunz, U. H. F.; Garcia-Garibay, M. A. *J. Am. Chem. Soc.* **2001**, *123*, 4259–4265. (f) McQuade, D. T.; Kim, J.; Swager, T. M. *J. Am. Chem. Soc.* **2000**, *122*, 5885–5886. (g) Levitsky, I. A.; Kishikawa, K.; Eichhorn, S. H.; Swager, T. M. *J. Am. Chem. Soc.* **2000**, *122*, 2474–2479. (h) Yeh, H.-C.; Yeh, S.-H.; Chen, C.-T. *Chem. Commun.* **2003**, 2632–2633.



**Figure 7.** Perspective view of the packing of gold complex **10a** in crystalline phase. H atoms are omitted for clarity.

makes a large contribution to the nonradiative transition process in solution. It is likely that a similar explanation can be invoked for phosphole-based fluorophores. Overall, these results nicely illustrate that the use of novel heterocyclic building blocks (siloles, phospholes...) can induce rather unusual photophysical properties.

It is interesting to note that the P chromophores depicted in Scheme 1 have different physical properties depending on their molecular structure. For example, their maximum emission wavelengths ( $\lambda_{em}$ ) in the solid state range from 517 to 553 nm, and both their oxidation and their reduction potentials vary by 0.4–0.5 eV (Table 2). This tuning is promising for OLED development because it would allow the emission color of the devices to be variant and also to reach a good match between the LUMO and HOMO levels and the work functions of electrodes. Unfortunately, the oxidation and reduction potentials were irreversible, so we cannot estimate their HOMO and LUMO energies reliably.

The results presented above show that the tuning of the electronic properties of phosphole-based oligomers by chemical modifications of the P center is a key point toward the development of these novel  $\pi$ -conjugated materials for OLEDs. To further exploit this unique capability, metal complexes were investigated, because phospholes act as 2-electron donors toward a wide range of transition metals.<sup>21</sup> In a first approach, Au(I) complexes were selected for two main reasons. First, despite the numerous studies on electroluminescent metal complexes,<sup>22</sup>

OLEDs based on luminescent Au(I) complexes have few precedents in the literature.<sup>23</sup> Second, Au(I) complexes have a strong tendency to form metal–metal interactions (aurophilicity) arising from correlation effects that are enhanced by a relativistic effect.<sup>24</sup> Au(I) complexes can thus self-associate in the solid state leading to luminescent aggregates.<sup>25</sup> Note that luminophores that can form aggregates with a broad spectral emission are of great interest for the development of white organic light-emitting diodes (WOLEDs),<sup>2e,25</sup> a promising device for lighting applications.<sup>2e</sup>

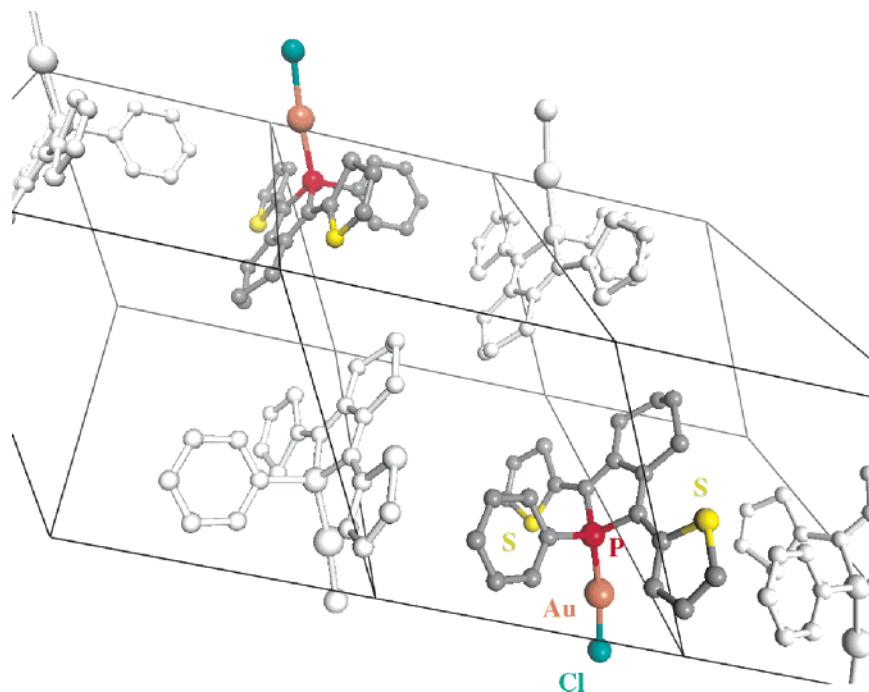
Phospholes **5a** and **5b** reacting in  $\text{CH}_2\text{Cl}_2$  solution at room temperature with (tetrahydrothiophene)AuCl gave rise to the corresponding complexes **10a** and **10b** (Scheme 1), which were isolated as air-stable powders in 77% and 90% yield, respectively. Coordination of the P atom to the gold center is evidenced by the downfield  $^{31}\text{P}$  NMR coordination shift ( $\Delta\delta \approx 26$  ppm). For both complexes, the simplicity of the  $^1\text{H}$  and  $^{13}\text{C}$  NMR spectra favors a symmetric structure. These NMR data discount a chelating P,S-coordination mode for ligand **5b**. The proposed structures were confirmed by X-ray diffraction studies (Tables 3 and 4, Figures 7 and 8). The bond lengths within the phosphole moiety are similar for both complexes and compared to those of the thioxophosphole derivatives **7a** and **9a** (Table 3). As expected, the P atoms are tetrahedral [ $\Sigma(\text{CPC angles})$ : **10a**, 309.5°; **10b**, 305.5°], and the two-coordinate Au(I) atoms have an almost linear geometry [P–Au–Cl angles: **10a**, 171.64°; **10b**, 174.63°]. This slight deviation from ideal linearity is typical

(21) (a) Leca, F.; Sauthier, M.; Deborde, V.; Toupet, L.; Réau, R. *Chem.-Eur. J.* **2003**, *9*, 3785–3795. (b) Leca, F.; Lescop, C.; Rodriguez, E.; Costuas, K.; Halet, J.-F.; Réau, R. *Angew. Chem., Int. Ed.* **2005**, *44*, 4362–4365. (c) Leca, F.; Sauthier, M.; Le Guennic, B.; Lescop, C.; Toupet, L.; Halet, J.-F.; Réau, R. *Chem. Commun.* **2003**, 1774–1775. (d) Leca, F.; Lescop, C.; Réau, R. *Organometallics* **2004**, *23*, 6191–6201. (e) Sauthier, M.; Leca, F.; Toupet, L.; Réau, R. *Organometallics* **2002**, *21*, 1591–1602. (f) Hay, C.; Sauthier, M.; Deborde, V.; Hissler, M.; Toupet, L.; Réau, R. *J. Organomet. Chem.* **2002**, *643–644*, 494–497. (g) Caballero, A.; Jalon, F. A.; Manzano, B. R.; Sauthier, M.; Toupet, L.; Réau, R. *J. Organomet. Chem.* **2002**, *663*, 118–126. (h) Sauthier, M.; Le Guennic, B.; Deborde, V.; Toupet, L.; Halet, J.-F.; Réau, R. *J. Organomet. Chem.* **2001**, *40*, 228–231.

(22) For recent examples, see: (a) Lu, W.; Mi, B. X.; Chan, M. C. W.; Hui, Z.; Che, M.; Zhu, N.; Lee, S. T. *J. Am. Chem. Soc.* **2004**, *126*, 4958–4971. (b) Lin, W.; Jen, A. K. Y.; Niu, U. H.; Zhang, L. *Chem. Commun.* **2005**, 1002–1004. (c) Liu, C. Y.; Bard, A. J. *J. Am. Chem. Soc.* **2002**, *124*, 4190–4191. (d) Welter, S.; Krunner, K.; Hofstraat, J. W.; De Cola, L. *Nature* **2003**, *421*, 54–57. (e) Baldo, M. A.; O'Brien, D. F.; You, Y.; Shoustikov, A.; Sibley, S.; Thompson, M. E.; Forrest, S. R. *Nature* **1998**, *395*, 151–154.

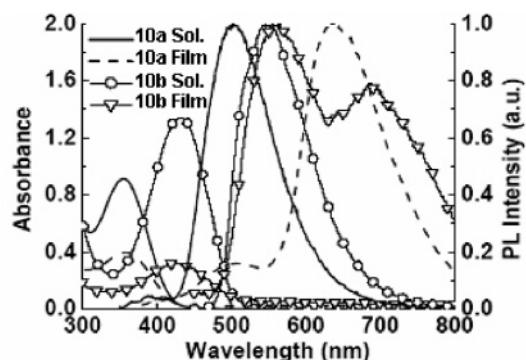
(23) For Au(I) complex-based OLEDs, see: (a) Ma, Y.; Zhou, X.; Shen, J.; Chao, H.-Y.; Che, C.-M. *Appl. Phys. Lett.* **1999**, *74*, 1361–1363. For Au(III) complex-based OLEDs, see: (b) Wong, K. M.-C.; Zhu, X.; Hung, L.-L.; Zhu, N.; Yam, V. W. W.; Kwok, H.-S. *Chem. Commun.* **2005**, 2906–2908.





**Figure 8.** Perspective view of the packing of gold complex **10b** in crystalline phase. H atoms are omitted for clarity.

of the sp hybridization of gold(I).<sup>24m</sup> The Au–P [2.2290(16), 2.2300(16) Å] and Au–Cl [2.2638(18), 2.2895(19) Å] distances are usual for two-coordinated gold(I) complexes.<sup>23m</sup> Two structural features are noteworthy. First, the diphenylphosphole moiety of complex **10a** exhibits an important rotational disorder (twist angles, 43.3–54.5°), whereas the three heterocycles of the di(2-thienyl)phosphole moiety of complex **10b** are almost coplanar (twist angles, 3.8–13.0°). Basically, these properties can increase the degree of conjugation in the thienyl-capped derivative **10b** as compared to **10a**. Second, the shortest distance between two Au(I) centers is 8.7 Å for **10a** and 9.0 Å for **10b**, and the interchromophore spacing is rather large (>5.2 Å). These large separation values clearly indicate the absence of any aurophilic or  $\pi$ – $\pi$  interactions in the crystal lattice (Figures 7 and 8).

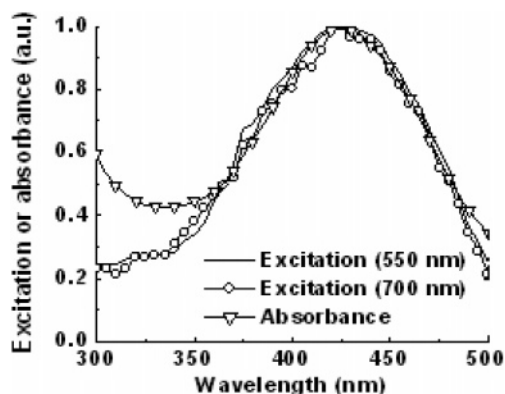


**Figure 9.** UV–vis and emission spectra of **10a** and **10b** in solution ( $\text{CH}_2\text{Cl}_2$ ) and in thin film.

In  $\text{CH}_2\text{Cl}_2$  solution, complexes **10a** and **10b** have a maximum absorption in the visible region, and, as observed in the thioxophosphole series, the value for the thienyl-capped complex **10b** is 70 nm red shifted as compared to that of its phenyl analogue **10a** (Table 2). On excitation at their  $\lambda_{\text{max}}$ , these gold complexes display one broad emission band in the greenish region (**10a**, 506 nm; **10b**, 544 nm, Figure 9) with absolute quantum yields varying from 7.3% (**10a**) to 12.9% (**10b**). The Stokes shifts (126–146 nm) lie within the range of those of thioxophospholes (116–167 nm), and the nanosecond lifetimes of the excited state indicate that the emission is due to fluorescence (Table 2). These data strongly suggest that the absorption and emission of gold complexes **10a,b** in solution are associated with metal-perturbed intraligand (IL)  $\pi$ – $\pi^*$  transitions of the 2,5-diarylphosphole ligands. It is noteworthy that the quantum yields of complexes **10a,b** are much higher than those of the corresponding thioxophospholes **7a,b** (Table 2), illustrating that the nature of the P modification has a considerable impact on the optical properties of these fluorophores.

Gold complexes **10a,b** are thermally stable enough ( $T_{\text{d}10} \geq 218^\circ\text{C}$ , Table 2) to give thin films upon vacuum sublimation.

- (24) (a) Schmidbaur, H. *Gold Bull.* **1990**, *23*, 11–21 (b) Scherbaum, F.; Grohmann, A.; Huber, B.; Krüger, C.; Schmidbaur, H. *Angew. Chem., Int. Ed. Engl.* **1988**, *27*, 1544–1546. (c) Pyykkö, P. *Chem. Rev.* **1997**, *97*, 597–636. (d) Jiang, Y.; Alvarez, S.; Hoffmann, R. *Inorg. Chem.* **1985**, *24*, 749–757. (e) Mingos, D. M. P. *J. Chem. Soc., Dalton Trans.* **1976**, 1163–1169. (f) Harwell, D. E.; Mortimer, M. D.; Knobler, C. B.; Anet, F. A. L.; Hawthorne, M. F. *J. Am. Chem. Soc.* **1996**, *118*, 2679–2685. (g) Narayanaswamy, R.; Young, M. A.; Parkhurst, E.; Ouellette, M.; Kerr, M. E.; Ho, D. M.; Elder, R. C.; Bruce, A. E.; Bruce, M. R. *Inorg. Chem.* **1993**, *32*, 2506–2517. (h) Zhang, H. X.; Che, C. M. *Chem.-Eur. J.* **2001**, *7*, 4887–4893. (i) Assefa, Z.; McBurnett, B. G.; Staples, R. J.; Fackler, J. P., Jr.; Assmann, B.; Angermaier, K.; Schmidbaur, H. *Inorg. Chem.* **1995**, *34*, 75–83. (j) Jones, W. B.; Yuan, J.; Narayanaswamy, R.; Young, M. A.; Elder, R. C.; Bruce, A. E.; Bruce, M. R. *Inorg. Chem.* **1995**, *34*, 1996–2001. (k) Forward, J. M.; Bohmann, D.; Fackler, J. P., Jr.; Staples, R. J. *Inorg. Chem.* **1995**, *34*, 6330–6336. (l) Hanna, S. D.; Zink, J. I. *Inorg. Chem.* **1996**, *35*, 297–302. (m) Li, C.-K.; Lu, X.-X.; Wong, K. M.-C.; Chan, C.-L.; Zhu, N.; Yam, V. W. W. *Inorg. Chem.* **2004**, *43*, 7421–7430. (n) Pyykkö, P. *Angew. Chem., Int. Ed.* **2004**, *43*, 4412–4456. (o) Yam, V. W. W.; Lo, K. K. W.; Fung, W. K. M.; Wang, C. R. *Coord. Chem. Rev.* **1998**, *171*, 17–41.
- (25) (a) D’Andrade, B. W.; Brooks, J.; Adamovitch, V.; Thompson, M. E.; Forrest, S. R. *Adv. Mater.* **2002**, *14*, 1032–1036. (b) Adamovitch, V.; Brooks, J.; Tamayo, A.; Alexander, A. M.; Durovitch, P. I.; D’Andrade, B. W.; Adachi, C.; Forrest, S. R.; Thompson, M. E. *New J. Chem.* **2002**, *26*, 1171–1178. (c) Feng, J.; Li, F.; Gao, W.; Liu, S.; Liu, Y.; Wang, Y. *Appl. Phys. Lett.* **2001**, *78*, 3947–3949. (d) D’Andrade, B. W.; Thompson, M. E.; Forrest, S. R. *Adv. Mater.* **2001**, *14*, 147–151. (e) Wang, L.; Lei, G.; Qiu, Y. *J. Appl. Phys.* **2005**, *97*, 114503–114508. (f) Yan, S.; Yang, Y. *Appl. Phys. Lett.* **2005**, *86*, 7351–7353.



**Figure 10.** Absorption and excitation spectra of **10b** in thin film recorded for emission.

The absorption spectra in solution or in thin film of these complexes are similar (Table 2, Figure 9). In marked contrast, the solution and thin-film emission spectra of the gold complexes are different. Two broad emission bands are observed for the thin films, one at a wavelength similar to that of the solution spectrum (**10a**, 505 nm; **10b**, 550 nm), and a second that is considerably red-shifted (**10a**, 630 nm; **10b**, 690 nm) (Figure 9). Note that the relative intensity of these two bands depends on the nature of the phosphole ligand. They have a comparable intensity for the thienyl-capped derivative **10b**, whereas for its phenyl analogue **10a** the long-wavelength band is far more intense (Figure 9). The lifetimes of the red-emitting species are longer than those of the higher-energy emitting species (Table 2), but they are still in the nanosecond range, suggesting that both emissions are due to fluorescence. The emission bands at shorter wavelength (**10a**, 505 nm; **10b**, 550 nm) can reasonably be assigned to IL  $\pi$ - $\pi^*$  transitions of site-isolated gold complexes because their positions closely match those recorded in dilute solution (Figure 9). The second emission band at longer wavelengths is not due to the formation of a new emitting species arising from chemical transformation of complexes **10a,b**, since we have checked that they do not decompose or transform upon sublimation under high vacuum ( $4 \times 10^{-5}$  Torr). Moreover, the excitation spectra of **10b** in thin film recorded for emission at 550 or 700 nm are similar to its absorption spectrum (Figure 10), clearly indicating that both emissions are due to the (phosphole)gold complexes. The second emission can also not be attributed to vibronic couplings or aggregation-induced planarization<sup>41</sup> because the energy difference between the two emissions is large ( $>4000$   $\text{cm}^{-1}$ ). Hence, the low-energy luminescence bands obtained in thin film with phosphole Au(I) complexes **10a,b** probably arise from the formation of aggregates. This hypothesis is supported by the fact that the low-energy emission bands are no longer observed when complexes **10a,b** are dispersed in a polymethylmetacrylate matrix. In this discussion, the term “aggregate” is used to describe both excited-state (excimer) and ground-state (oligomers) aggregated species arising from  $\pi$ - $\pi$  stacking and metal-metal interactions, respectively. The high-wavelength emissions are not due to metal-centered excited states (MC) because MCs involving Au centers are triplet in nature with microsecond lifetimes.<sup>24</sup> However, it is clear that the gold centers play a key role in the formation of these aggregates because no low-energy luminescence bands are observed with the thioxophosphole derivatives **7a,b** (Figure 6). It is striking to note that neither

aurophilic nor  $\pi$ - $\pi$  interaction is observed in the solid-state crystal structures of complexes **10a,b** (Figures 7 and 8). However, the films obtained by vacuum deposition do not exhibit long-range ordering, as revealed by the broad powder X-ray diffraction signal of complex **10b**. These data indicate that the bulk organization of the gold-coordinated phospholes depends on the conditions of solid formation and that crystalline structures are not always good models for amorphous thin films obtained by vacuum sublimation.<sup>20d,26</sup> Whatever the driving force for aggregate formation (aurophilic or/and  $\pi$ - $\pi$  interactions), thin films of complexes **10a,b** cover a broad range of the visible spectrum due to dual monomeric and aggregate emissions, a feature which may have some interesting implications for WOLED fabrication.

Hence, fine chemical tailoring based on the variation of the phosphole substituents and the nature of the P-modification afforded phosphole fluorophores with appealing properties. They are thermally stable enough to be sublimed, they form uniform thin films by vacuum deposition, and they exhibit different optical and electrochemical properties. The next step was therefore to evaluate these P-based oligomers as materials for OLEDs fabrication.

**OLEDs Incorporating Phosphole Derivatives.** Derivatives **6**, **7a,b**, **8a**, and **9a** (Scheme 1) were investigated as organic materials in single-layer OLEDs **A–E** (Table 5), having a ITO/PEDOT:PSS(25 nm)/organic layer/Mg:Ag(80 nm)/Ag(150 nm) configuration. Not surprisingly, the performances of each device are significantly dependent on the phosphole materials employed. The OLED device **A** displays greenish emission ( $\lambda_{\text{max}}^{\text{EL}} = 510$  nm) for a turn-on voltage of 6.0 V (Table 5). The electroluminescence spectrum (EL) of the device resembles the thin-film PL of **6** (Figure 11), showing that the EL emission band is from the  $\sigma^3$ -phosphole derivative **6**. The maximum brightness attains 1000  $\text{cd m}^{-2}$ , but the EL quantum yield is low (Table 5). With relatively low turn-on voltages (2.0–3.6 V), devices **B** and **C** emit green to yellow light ( $\lambda_{\text{max}}^{\text{EL}}$ : **B**, 531 nm; **C**, 557 nm) with a broad emission band (full width at half-maximum of ca. 100 nm) (Table 5). The EL spectra of these devices **B** and **C** match those of the solid-state PL spectra of the  $\sigma^4$ -thioxophospholes **7a** and **7b** (Figure 12), respectively, indicating similar mechanisms for both types of emission. As expected from the thin-film study, no low-energy emission arising from exciplex is observed. The maximum brightness ( $B_{\text{max}}$ ) and external EL quantum efficiency (EEQE) are by far higher with the thienyl-capped phosphole **7b** than for its phenyl analogue **7a** (Table 5, **C** versus **B**). Devices **D** and **E** also exhibit a single broad PL emission, which matches those of the  $\sigma^4$ -thioxophosphole materials **8a** and **9a**, respectively (Table 5). Here also, the turn-on voltages are rather low (2.2–3.2 V), the  $B_{\text{max}}$ 's are satisfactory, and yet the EEQE's are low (Table 5). Overall, these results show that  $\pi$ -conjugated oligomers containing  $\sigma^3$ - or  $\sigma^4$ -phosphole moieties can be employed as multifunctional materials in single-layer OLEDs.

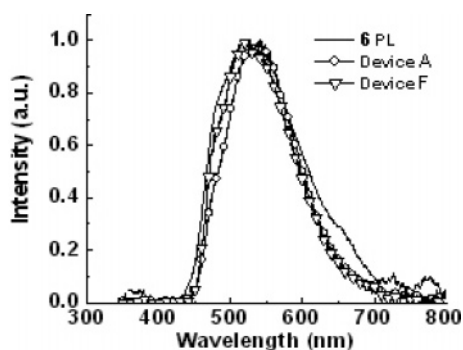
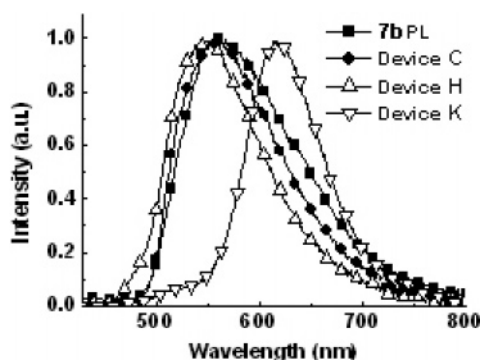
One appealing property of these P-materials is that, as expected from the data recorded in thin film (Table 2), the  $\lambda_{\text{em}}$  values of the OLEDs vary with the nature of the phosphole derivative (Table 5). Among devices **A–E**, the best performances in all aspects are obtained with **C** including the bis(2-

(26) Van Hutten, P. F.; Krasnikov, V. V.; Hadzioannou, G. *Acc. Chem. Res.* **1999**, *32*, 257–265.

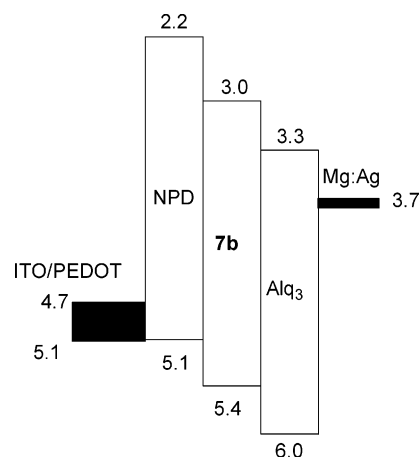
**Table 5.** Electroluminescence Characteristics of Devices A–Q

device	organic layer [nm] <sup>a</sup>	$\lambda_{\text{max}}^{\text{EL}}$ [nm]	$V_{\text{on}}^b$ [V]	$V_{20}^c$ [V]	$V_{\text{max}}^d$ [V]	$B_{20}^e$ [cd m <sup>-2</sup> ]	$B_{\text{max}}^f$ [cd m <sup>-2</sup> ]	$\eta_{20}^g$	$\eta_{\text{max}}^h$	$\text{lm}/W_{20}^i$	$\text{lm}/W_{\text{max}}^j$
A	6(80)	510	6.0	14.0	16.1	150	1000	0.07	0.08	0.056	0.056
B	7a(60)	531	3.6	2.8	10.0	$3.4 \times 10^{-4}$	5.7	$6.9 \times 10^{-5}$	0.048	$1.8 \times 10^{-6}$	$4.8 \times 10^{-3}$
C	7b(75)	557	2.0	4.5	8.0	50	3613	0.09	0.16	0.175	0.222
D	8a(50)	528	3.2	7.6	10	7.2	76.5	0.01	0.014	0.015	0.016
E	9a(18)	524	2.2	3.7	7.2	6.5	692	0.009	0.017	0.024	0.035
F	$\alpha$ -NPD(40)/6(40)/Alq <sub>3</sub> (20)	510	4.0	8.5	12.2	500	5600	0.27	0.29	0.33	0.37
G	$\alpha$ -NPD(40)/7a(20)/Alq <sub>3</sub> (40)	567	3.2	9.2	10.0	26.6	57	0.05	0.21	0.047	0.20
H	$\alpha$ -NPD(40)/7b(20)/Alq <sub>3</sub> (40)	550	2.2	8.5	15.0	450	37 830	0.74	0.80	0.827	1.14
I	$\alpha$ -NPD(40)/8a(20)/Alq <sub>3</sub> (40)	544	3.2	9.4	10	84	152	0.14	0.14	0.13	0.29
J	$\alpha$ -NPD(40)/9a(20)/Alq <sub>3</sub> (40)	549	2.6	7.9	10	188	2110	0.32	0.32	0.37	0.59
K	$\alpha$ -NPD(40)/7b:DCJTB(20)/Alq <sub>3</sub> (40) <sup>k</sup>	617	2.4	8.0	13.5	530	36 538	1.83	1.83	1.12	1.61
L	$\alpha$ -NPD(40)/Alq <sub>3</sub> :DCJTB(20)/Alq <sub>3</sub> (40)	613	2.2	8.6	15.0	780	50 719	2.20	3.70	1.40	6.0
M	10a(71)	640	14	16.2	20.0	0.20	1.2	0.021	0.025	$4.3 \times 10^{-3}$	$6.5 \times 10^{-3}$
N	10b(56)	565	4.0	7.8	10.0	0.15	2.6	$3.7 \times 10^{-4}$	$2.7 \times 10^{-4}$	$3 \times 10^{-4}$	$1.7 \times 10^{-3}$
O	$\alpha$ -NPD(40)/10a(40)/Alq <sub>3</sub> (20)	637	9.0	12.0	22.0	0.50	60	0.045	0.05	$7.5 \times 10^{-3}$	$8.5 \times 10^{-3}$
P	$\alpha$ -NPD(40)/10b(20)/Alq <sub>3</sub> (40)	540	2.2	10.0	16.0	180	2786	0.35	0.36	0.28	0.39
Q	$\alpha$ -NPD(40)/10b:DCJTB(20)/Alq <sub>3</sub> (40) <sup>k</sup>	623	2.2	10.5	15.5	200	36 538	0.67	1.22	0.30	1.02

<sup>a</sup> Device configurations (thickness): ITO/PEDOT:PSS(25/nm)/organic layer/Mg:Ag(80/nm)/Ag(150/nm). <sup>b</sup> Turn-on voltage at which emission becomes detectable ( $\sim 10^{-4}$  cd m<sup>-2</sup>). <sup>c</sup> Voltage for a current density of 20 mA cm<sup>-2</sup>. <sup>d</sup> Voltage at the maximum brightness ( $B_{\text{max}}$ ). <sup>e</sup> Brightness at  $V_{20}$ . <sup>f</sup>  $B_{\text{max}}$ . <sup>g</sup> External EL quantum efficiency (EELQ) at 20 mA cm<sup>-2</sup>. <sup>h</sup> Maximal EELQ. <sup>i</sup> Luminous efficiency (LE) at 20 mA cm<sup>-2</sup>. <sup>j</sup> Maximal LE. <sup>k</sup> DCJTB 1.4 wt %.

**Figure 11.** PL spectrum of **6** in thin film and EL spectra of devices A and F.**Figure 12.** PL spectrum of **7b** in thin film and EL spectra of devices C, H, and K.

thienyl)thioxophosphole **7b** as the multifunctional organic layer. The EL is obtained with a low turn-on voltage (2.0 V), and the maximum brightness reaches 3613 cd m<sup>-2</sup>. However, the EL quantum yield is modest (0.16%), presumably due to unbalanced carrier injection and/or transport. Single-layer OLEDs usually give poor efficiency and brightness because EL organic materials tend to have either p-type (hole-transport) or n-type (electron-transport) charge-transport characteristics.<sup>2,3</sup> The experimental determination of IP and EA values for organic materials is difficult. It has been suggested by Jenekhe et al. that a fair estimation of IP and EA can be derived from cyclic voltammetry by taking  $\text{EA(eV)} = E_{\text{onset}}^{\text{red}}(\text{vs SCE}) + 4.4$  and

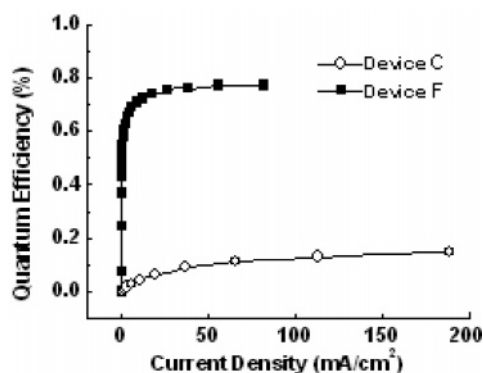
**Figure 13.** Relative energy level diagram for device F.

$\text{IP(eV)} = E_{\text{onset}}^{\text{ox}}(\text{vs SCE}) + 4.4$ .<sup>2c</sup> If one considers work functions  $\phi_c = 3.70$  eV for the Mg:Ag cathode and  $\phi_a = 5.10$  eV for the ITO/PEDOT anode,<sup>27</sup> these data show rather large barriers for electron injection for phosphole-based materials ( $\phi_c - \text{EA} \approx 0.7\text{--}1.1$  eV). The barriers for hole injection are lower ( $\phi_a - \text{IP} \approx 0.2\text{--}0.7$ ), indicating an unbalanced carrier injection.

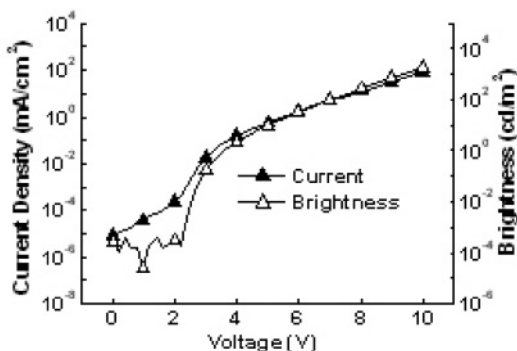
To further improve device characteristics, multilayered devices F–J in which the phosphole layer is sandwiched between a hole-transport layer ( $\alpha$ -NPD, Figure 2) and an electron-transport layer (Alq<sub>3</sub>, Figure 2) were prepared. Figure 13 shows schematically the energy-level diagram<sup>4c</sup> for one of the multilayer devices, from which one may expect reduced barriers for carrier injection and thus improved device characteristics. The EL spectra of devices F–J are similar to those of the corresponding single-layer OLEDs A–E (Figures 11 and 12), suggesting that the EL emission arises purely from the phosphole materials. The turn-on voltages required to drive multilayer devices are lower (A/F, B/G, Table 5) or comparable to those of the corresponding single-layer OLEDs. The external EL quantum efficiency (EELQ) and brightness of the multilayer devices are dramatically superior to those of their single-layer

(27) (a) Gu, G.; Bulovic, V.; Burrows, P. E.; Forrest, S. R.; Thompson, M. E. *Appl. Phys. Lett.* **1996**, *68*, 2606–2608. (b) Burrows, P. E.; Gu, G.; Forrest, S. R.; Vincenzi, E. P.; Zhou, T. *J. Appl. Phys.* **2000**, *87*, 3080–3085.





**Figure 14.** Comparison of external EL quantum efficiency versus current density for devices C and F.

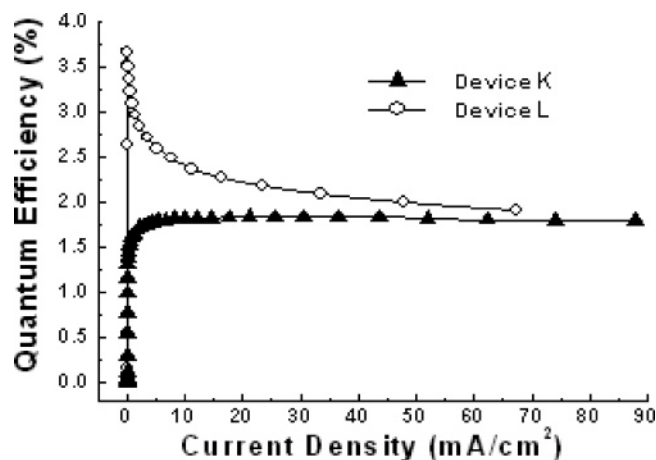


**Figure 15.** Current density and brightness versus voltage for device F.

counterparts (Table 5). For example, with **7b**, the maximum brightness is enhanced by 1 order of magnitude (C/H, 3613/37830  $\text{cd m}^{-2}$ ) and the maximum EELQ is multiplied by 5 (C/H, 0.16/0.80). The higher efficiency of multilayer over single-layer OLEDs is further illustrated in Figure 14, which compares the external EL quantum efficiency of devices C and H versus current density. The current density–voltage–brightness characteristics of device H are presented in Figure 15.

This first report on the use of EL organophosphorus derivatives proves that there is no inherent limit to the development of P-containing conjugated systems for optoelectronic functions. Furthermore, these results demonstrate that exploiting the reactivity of the P center of phosphole-based oligomers is a clue to optimizing these materials. Hence, it is clear that there is plenty of room for further improvement of the OLED performances through structural modifications of these phosphole-based materials.

Another effective way to further improve OLED performance, and also to tune their color, is to dope highly fluorescent dyes as guests into an emissive host matrix.<sup>2</sup> This guest–host doped emitter system is widely used for solving the problem of red-emissive materials being prone to aggregation in the solid state.<sup>2d</sup> 2,5-(2-Dithienyl)thioxophosphole **7b** was thus evaluated as the host material for DCJTB (Figure 2), one of the best red-emitting dopants for OLEDs.<sup>2d</sup> The testing device **K** has the same configuration of multilayer device **H** except for 1.4 wt % of DCJTB doped in the organic layer of **7b** (Table 5). The dopant concentration was not optimized, although the effective dopant range can be narrow. Device **K** showed red emission from DCJTB (Figure 12), indicating effective resonant energy transfer (Förster resonance) or carrier trapping from **7b** to DCJTB. Moreover, this new device is more efficient than the corre-



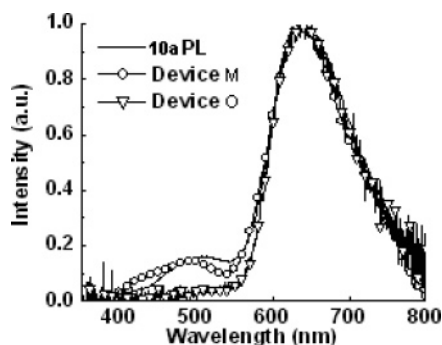
**Figure 16.** External EL quantum efficiency versus current density for devices K and L.

sponding “nondoped” device **H** (Table 5). Upon doping with DCJTB, the turn-on voltage and maximal brightness remain similar (Table 5, devices **H/K**), but the EL efficiency increases from 0.74% to 1.83% photon/electron and the luminous efficiency from 0.83 to 1.12 lm/W. One of the major concerns for practical applications of OLEDs is the current-induced luminescence quenching, particularly in red OLEDs.<sup>2</sup> We therefore studied the current–density dependence of the device efficiency. The external EL quantum efficiency of device **K** is unaffected by the driving current density in the range of 0–90  $\text{mA/cm}^2$  (Figure 16). This behavior is promising, because the efficiency of the conventional DCJTB-doped Alq<sub>3</sub> devices usually decays rapidly upon increasing the driving current due to quenching effects of charged excited states of Alq<sub>3</sub> on red dopants.<sup>2,28</sup> This behavior is illustrated by the DCJTB(1.4%)-doped Alq<sub>3</sub> device **L** consisting of ITO/PEDOT:PSS(25 nm)/ $\alpha$ -NPD(40 nm)/Alq<sub>3</sub>:DCJTB(20 nm)/Alq<sub>3</sub>(40 nm)/Mg:Ag(80 nm)/Ag(150 nm) (Figure 16). To circumvent this problem, which affects reliability and lifetime of a DCJTB-doped device, an assisting dopant (rubrene, quinacridone...) was added in the fabrication of some reported device.<sup>2d,27a,d</sup> The role of these assisting dopants is to reduce the formation of [Alq<sub>3</sub>]<sup>•+</sup>, which is a well-known quenching species for red-emitting dopants.<sup>28e,f</sup> Thus, 2,5-di(2-thienyl)thioxophosphole **7b** appears to be an attractive host material for DCJTB, because it solves the problem of luminescence quenching at high drive current without using the more complicated assisting-dopant technique. This is an important feature because the stability in EL quantum efficiency and color over a wide range of current density is crucial for OLED applications that require high current density (i.e., passive matrix displays, solid-state lasers...).

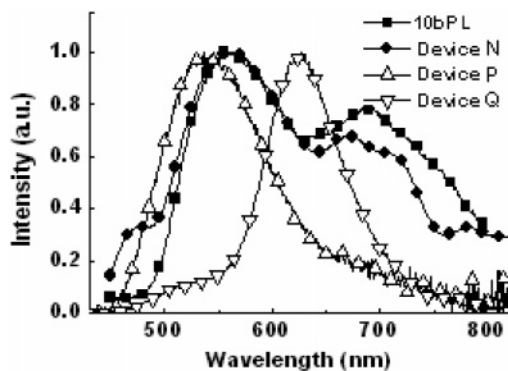
Similarly, gold complexes **10a** and **10b** were subjected to EL studies using also the single-layer structure (devices **M** and **N**, Table 5) and the multilayer structure (devices **O** and **P**, Table 5). Figures 17 and 18 compare the thin-film PL and EL spectra of **10a** (devices **M** and **O**) and **10b** (devices **N** and **P**), respectively. As observed for thin-film PL of **10a** and **10b**, their

(28) (a) Liu, T.-H.; Iou, C.-Y.; Chen, C. H. *Appl. Phys. Lett.* **2003**, *83*, 5241–5243. (b) Young, R. H.; Tang, C. W. *Appl. Phys. Lett.* **2002**, *80*, 874–876. (c) Feng, J.; Li, F.; Gao, W.; Cheng, G.; Xie, W.; Liu, S. *Appl. Phys. Lett.* **2002**, *81*, 2935–2937. (d) Xie, Z. Y.; Hung, L. S.; Lee, S. T. *Appl. Phys. Lett.* **2001**, *79*, 1048–1050. (e) Young, R. H.; Tang, C. W.; Marchetti, A. *Appl. Phys. Lett.* **2002**, *80*, 1465–1467. (f) Young, R. G.; Tang, C. W.; Marchetti, A. P. *Appl. Phys. Lett.* **2002**, *80*, 874–876.





**Figure 17.** PL spectrum of **10a** in thin film and EL spectra of devices **M** and **O**.



**Figure 18.** PL spectrum of **10b** in thin film and EL spectra of devices **N**, **P**, and **Q**.

EL spectra also show two broad emission bands, suggesting similar emission mechanisms for both PL and EL. With **10a** as the emitting material, the long-wavelength band (around 630 nm) is dominant, and the devices gave rather saturated red emission (Table 5). The CIE (Commission Internationale de l'Eclairage) 1931 color chromatography coordinates of device **M** are  $x = 0.61$  and  $y = 0.39$ , close to those of the standard red CRT Phosphors of the Society of Motion Picture and Television Engineers ( $x = 0.64$ ,  $y = 0.34$ ). Note that nondoped red OLEDs are relatively rare.<sup>2d,20d</sup> Using **10b**, the relative intensity of the long-wavelength band varies with the device structures, which may be due to optical effects (e.g., reflection, interference, etc.) of the device structure on emitting species at different locations. It is interesting to note that in the single-layer device of **10b**, the EL spectrum covers uniformly a broad spectral range of 500–800 nm due to the well-balanced dual monomer and aggregate emissions (Figure 18). Once again, these results underline that the properties of phosphole-based materials can be tuned through specific chemical modifications of the P atom. As in previous cases, incorporating the hole-transport layer and the electron-transport layer to form the multilayer devices **O** and **P** also significantly enhances the efficiencies and brightness of devices (Table 5). Here also, the best performances are obtained with the thienyl-substituted phosphole derivative (device **P**). The OLED using the di(2-thienyl)phosphole-gold complex **10b** shows a low turn-on voltage (2.2 V); the external EL quantum efficiency and the maximum brightness reach 0.36% and 2786 cd/m<sup>2</sup>, respectively. Complex **10b** was also evaluated as the host material for DCJTb in multilayer device **Q** with a 1.4 wt % DCJTb doped in the organic layer of **10b** (Table 5). Device **Q** showed red emission from DCJTb (Figure 18), even though **10b** itself has emission states of even lower

energies. Such results indicate that with DCJTb doping, the transition from the high-energy emission states of **10b** to the lower-energy emission states of **10b** is rather suppressed by the effective transfer to DCJTb excited states. The emission efficiency of this device **Q** is markedly enhanced as compared to device **P** (Table 5); its external EL quantum efficiency and maximum brightness reach 1.22% and 36 538 cd/m<sup>2</sup>, respectively.

## Conclusion

The phosphole-based EL materials presented in this work possess appealing properties such as ease of synthesis and purification, thermal stability, and enhancement of PL efficiency in the solid state. Moreover, they are attractive because of the flexibility available for fine-tuning their electronic properties through the manipulation of their chemical structures. This is nicely illustrated by the fact that the nature of the P moiety affects the bulk molecular environment and hence the photo-physical behavior of these chromophores in the solid state; thioxophosphole derivatives are isolated luminophores, whereas gold(I) phosphole complexes form aggregates leading to broad emission spectra from both monomer and aggregate states. This dichotomy shows that the presence of reactive P atoms allows for a unique molecular design to vary and to control the electronic structures of  $\pi$ -conjugated materials. Moreover, we have shown that  $\sigma^3$ - and  $\sigma^4$ -phosphole-based conjugated oligomers can act as multifunctional materials for OLEDs. Single- and multilayer OLEDs have been prepared, and a color tuning was achieved by the proper selection of the phosphole substituents. Di(2-thienyl)thioxophosphole **7b** appeared to be the most efficient P material in many respects. Of particular interest, it is a host for the fabrication of red OLEDs stable over a wide range of current densities, which is important for display and solid-state lighting applications. OLEDs using phosphole complexes **10a,b**, which are among the rare gold(I) complexes used for this type of application, cover broad emission spectra due to EL from monomer and aggregate states. This property can be of interest for future development of WOLEDs based on a single emissive material. The results presented in this paper are the basis for further development of P materials for optoelectronic applications because they show that there is no inherent impossibility in using organophosphorus moieties to construct functional materials. Furthermore, they demonstrate the versatility provided by the exploitation of P chemistry in this field. It can be expected that, besides the classic applications of organophosphorus derivatives (ligands design, medicinal chemistry...), more and more P materials featuring different moieties (Figure 1) and optoelectronic functions will emerge soon.

**Acknowledgment.** We thank the Ministère de l'Éducation Nationale, de la Recherche et de la Technologie, the Institut Universitaire de France, the Centre National de la Recherche Scientifique, and the National Science Council of the Republic of China for financial support. Thanks are due to Christophe Lescop for X-ray diffraction studies.

**Supporting Information Available:** Experimental, spectroscopic, and other experimental details of new compounds, table of crystallographic data, structure refinement details, atomic coordinates, interatomic distances and angles, and anisotropic displacement parameters (CIF). This material is available free of charge via the Internet at <http://pubs.acs.org>.

JA0567182